

Preparation of magnetic methotrexate nanocarrier coated with extracted hydroxyapatite of sea urchin (*Echinometra mathaei*)

Ali Rajabiyani^a, Nader Shakiba Maram^b, Ebrahim Rajabzadeh Ghatrami^c and Amanollah Zarei Ahmady^{b,*}

^aMarine Pharmaceutical Science Research Center, Ahvaz Jundishapur University of Medical Sciences, Ahvaz, Iran

^bNanotechnology Research Center, Ahvaz Jundishapur University of Medical Sciences, Ahvaz, Iran

^cDepartment of Fisheries, Faculty of Marine Natural Resources, Khorramshahr University of Marine Sciences and Technology, Khorramshahr, Iran

Abstract. New polymer-coated magnetic nanocarrier using magnetic iron oxide nanoparticles coated with chitosan and nanohydroxyapatite extracted from Sea urchin that both have anti-cancer properties showed good ability to Methotrexate (MTX) delivery. Iron oxide nanoparticles and hydroxyapatite prepared by co-precipitation and hydrothermal methods respectively. To stabilize the nanoparticles and optimization of the nanoparticles with hydroxyapatite, 3-chloropropyltriethoxysilane and chitosan were performed. The water-soluble anticancer drug Methotrexate was selected as the drug model. The drug loading percentage was %86.66, loading efficiency was %99.5 and the polydispersity of the nanoparticles was 0.01. The kinetic pattern of drug release is consistent with the Peppas equation and the results of the thermal analysis confirm the stability of the crystalline form of the drug. The FTIR results and FE-SEM images showed that the nanoparticles were successfully prepared and coated and their size ranged from 30 nm to 1.5 μm . The VSM analysis confirms the magnetic properties of the nanoparticles and the magnetic indices for the magnetic nanocarrier and the magnetic nanocarrier carrying MTX are 23 and 19 emu/g^{-1} , respectively. The present study demonstrates the potential of iron oxide nanoparticles for the design of new magnetic nanocarrier and for guiding Methotrexate drug therapy in cancer chemotherapy.

Keywords: Sea urchin, Fe_3O_4 nanoparticles, hydroxyapatite, methotrexate, drug delivery

1. Introduction

Nanoscience is now considered one among modern science's most vital areas of research and development. Within the latest years, nanotechnology study, specially engineered nanomaterials, has gained significant attention thanks to the introduction of fresh and enhanced technology. Engineered nanomaterials like carbon nanotubes, quantum dots, and magnetic nanoparticles are among the fore-

*Corresponding author: Amanollah Zarei Ahmady, Nanotechnology Research Center, Ahvaz Jundishapur University of Medical Sciences, Ahvaz, Iran. Tel.: +98 61 33115940; E-mail: zareia-ajums.ac.ir.; ORCID Number: 0000-0001-9315-9149

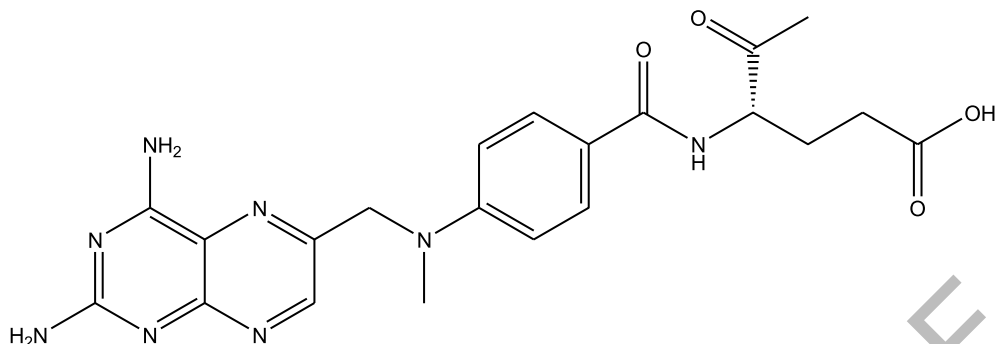


Fig. 1. Chemical structure of Methotrexate (6).

most promising materials used as vital platforms for targeted drug delivery, imaging, and therapeutic effectiveness tracking [1].

Methotrexate is (2S)-2-[(4-[(2,4-Diaminopteridin-6-yl)methyl](methyl)amino]benzoyl)amino]pentanedioic acid, consist of three main regions in its structure; pteridine ring, p-aminobenzoic acid (the bridge region) and glutamic acid (Fig. 1). Each of these regions has been varied in structure in many attempts to develop better inhibitors of DHFR for chemotherapeutic purposes [2].

Folic acid chemical structure is similar to methotrexate differing in the pteridine ring (by substitution of a hydroxyl group for an amine) and on the 10th nitrogen of p-aminobenzoic acid (by addition of a methyl group) [3]. Due to structural similarities, cells internalize MTX through a transport mechanism similar to that of folates, which inhibits the reduction of dihydrofolate (DHFR), a critical folic acid cycle enzyme and key to regulating homeostasis which leads to reduced cell viability and mortality from cells. As folate receptors are over-expressed in cell membranes of many cancer cells, MTX has been shown to be a strong anti-cancer agent [4]. In the treatment of autoimmune diseases, strong tumors, and hematological malignancies, MTX is well recognized among an anti-cancer drug. Although it's documented that MTX is in use in clinical cancers, its clinical efficacy is often limited due to its very brief plasma half-life, bad pharmacokinetics, susceptibility to patient medication resistance, and possible elevated dosages for chemical treatment. For the efficient deliverance of MTX, several studies are undertaken within the drug delivery community to enhance the pharmacokinetics and drug efficacy, blood circulation, controlled release, and therapeutic windows, also in overcoming drug resistance. Furthermore, hybridizing MTX with nanocarriers could open up fresh nanomedicine advances [5].

Several nano-carriers (e.g., magnetic nanoparticles, gold, and quantum dots) were implemented to develop within the distribution systems of MTX, including carbon nanotubes, polymer Nanoparticles (e.g. micelles, hydrogels), dendrimers, metal nanoparticles [7]. In other biomedical applications, iron oxide magnetic particles (IOMP) are of considerable concern, including clinical applications like cancer magnet hyperthermia, MRI, and drug releases. It is necessary to precoat the magnetic particles with materials that ensure their stability, biodegradability, and non-physiological toxicity. Simple Ferro/Ferrimagnetic particles are stable colloidal systems that are surfactant coated and spread into a container liquid. The biocompatible ferrofluids are often used as anti-cancer devices within the local tumor area, also as in magnetic therapy of hyperthermia [8].

A variety of coatings, like polyvinyl alcohol (PVA), chitosan (CS), Hydroxyapatite (HA), poly(ethylene glycol) (PEG), and starch are often used counting on apps [9]. the utilization of natural biopolymers like dextran, chitosan, etc. as stabilizers is more stable and biocompatible and therefore the surface are often modified with many various molecules, counting on how a variety of biomedical applications are required [10]. The coating material should have locations for the adsorption of the

drug molecules for adequate and effective drug delivery. These locations are often given mesoporous materials with distinctive tunable pores, a greater floor, and relatively big pore quantity [1].

The scientists have excellent interest within their prospective applications in the biomedical sector due to their simple access and sustainable exploitation in natural marine products, including agar, alginates, carrageenan, Chitin, and hydroxyapatite. Given its biodegradable and bioactive characteristics, it's been noted among several marine biomaterials. Chitosan has been wont to treat various medical applications, including aqueous solutions for drug use, tissue technology, wound dressings, antibacterial coatings, and separating membranes, and may be a non-poisonous, biocompatible and biodegradable amino polysaccharide. Chitosan is that the deacetylated derivative of chitin as a natural polymer, which is an organic matrix of arthropods and mollusks endoskeletons [11].

HA is that the main inorganic element of human bones and teeth with the molecular formula $\text{Ca}_{10}(\text{PO}_4)_6(\text{OH})_2$; it is abundant in nature, readily accessible, low cost, and features a minimal environmental impact in restoring or remediating the natural resources [12]. use It extends to another biomedical fields, like bone tissue engineering, drug delivery controlled, biomedical cover, gene therapy, wound treatment, and elsewhere [13]. HA compounds are obtained synthetically and naturally. It is often produced employing a range of techniques including hydrothermal synthesis, sol-gel, wet-chemical precipitation, and therefore the handling of a microwave [14]. The extraction from natural resources is an alternate technique for preparing HA. Corals, eggshells, echinoderm, and bovine bone, for instance, are utilized in the HA production [15].

Sea urchins part of speech Echinoidea within Echinodermata alongside their close relatives the heart urchins and sand dollars [16]. Echinoidea may be a taxonomic category of marine animals, frequently referred to as sea urchins, which is analogous to a physically-appeared hedgehog with spines that cover the body. The spines contains calcium and are brief, medium, and long [17]. Sea urchins are present altogether of the world's oceans, in environments starting from intertidal zone to quite 5000 m deep. Most species live in relatively shallow tropical or temperate waters [18]. Echinoderm habitats include the reef and rocky shores with seaweed and vary in color between species like brown, black, purple, green, white, or red. They also play a big role in regulating vegetation development within the ocean as they consume seaweed and scrap the benthic microalgae within the marine environment [19]. Urchins are defined by the fusion of the calcite ossicles (panels) and tails radiating from the test with five-fold symmetry, a collagenous dermis overlying an endoskeleton (test). Most of their spines are long and sharp, because they protect themselves against degradation. Spines up to a length of 30 cm and a diameter of up to 1 cm [20].

The aim of this study is to synthesize iron oxide nanoparticles, coat them with hydroxyapatite then characterize them for his or her possible application within the drug delivery. During this paper, natural HA was utilized in the preparation of composite structures instead of synthesized types. Natural HA was extracted from the ocean urchin shells. Therefore, it's less expensive than synthetic HA.

2. Material and methods

2.1. Materials and reagents

Sigma-Aldrich and Merck were the companies that chemicals were purchased from. HA was extracted from the sea urchin shells. MTX was obtained from BBI (USA), Chitosan powder (biomedical grade, viscosity average molecular 34×10^4 , degree of deacetylation is about 91%). orthophosphoric acid (H_3PO_4), ferrous chloride tetrahydrate ($\text{FeCl}_2 \cdot 4\text{H}_2\text{O}$), ferric chloride hexahydrate ($\text{FeCl}_3 \cdot 6\text{H}_2\text{O}$), Ammonium hydroxide, acetic acid solution, (3-chloropropyl)triethoxysilane (CPTES), Dimethyl sulfoxide (DMSO), N, N-dicyclohexylcarbodiimide (DCC), 4-dimethylaminopyridine (DMAP), Ethanol, Toluene, Acetone, deionized water, HCl of 1 M and Sodium hydroxide of 2 M are used to adjust the

pH of the environment. All chemicals were analytical grade reagents and used directly without further purification.

2.2. Methodology

2.2.1. Sample preparation

Sea Urchin of E. Matthaei was collected manually at depth 10 m from coastal waters of the port city of Souza, Persian Gulf (26°46'51" N and 56°03'47" E) in June 2018. To determine the classification of sea urchin by genus and species, the sea urchin appearance characteristics were examined and matched with a regional identification key (Price, 1983) to work out the sex and sort of species used. Samples are frozen and carried into the laboratory. The specimens were first dissected and their internal organs removed. The sea urchin shells were then washed twice with cold water to desalt. They were placed during a freeze-dryer at -40°C for twenty-four hours to dry and take away moisture.

2.2.2. Hydroxyapatite extraction from the Sea Urchin shells

The specimens were crushed with a grinding machine to obtain Aragonite soft powder. the method of extraction followed was consistent from the report by Komalakrishna et al. [21]. Then calcination of aragonite was administered to at 900°C to get CaO. Calcined powder (CaO) was dissolved in water and placed on a magnetic stirrer at 80°C and also the orthophosphoric acid (H₃PO₄) was added dropwise, maintaining a continuing stirring to take care of a stoichiometric calcium/phosphate molar ratio of 1.667. It had been stirred at 200 rpm for two hours for the successful completion of the reaction. Then the ultimate product was kept during a hot air oven at 100 °C overnight to get rid of the moisture content. Finally sintering at 1100 °C for 2 hours within the furnace.

2.2.3. Synthesis of Fe₃O₄ nanoparticles

Magnetic iron oxide nanoparticles were prepared by co-precipitation method [22]. Thus, 0.98 g of FeCl₂.4H₂O and 2.70 g of FeCl₃.6H₂O powder with a molar ratio of 1:2 are dissolved separately in 10 ml of deionized distilled water; both are transferred in a 100 ml balloon It was immersed in an oil bath and heated under nitrogen for 30 min at 80°C. Then 6 ml of ammonia 28% by weight drop was added to the above mixture and continued stirring under the nitrogen atmosphere for another 30 minutes. During the process of adding ammonia, the solution gradually changed from orange to brown and then to black. Indicating the formation of Fe₃O₄ nanoparticles. Upon reaching room temperature, the black precipitates were separated by a 1.4 Tesla magnet and washed several times with deionized distilled water. The precipitate was dried with a freeze dryer device and stored in a desiccator for later use.

2.2.4. Synthesis of Fe₃O₄/nHA nanoparticles

For synthesizing Fe₃O₄/nHA, 1.052 g of hydroxyapatite dissolve in 100 ml of distilled water and then drop the dropper add into a solution of 0.232 g Fe₃O₄ in 100 ml of distilled water. The solution stirs about 30 min by electric stirrer and adds 0.1 M of NaOH to pH 13. This mixed solution was stirred for about 6 hours by an electric stirrer. Precipitate was collected by magnet and washed several times with distilled water and dried in an oven at 50°C for 18 hours [23].

2.2.5. Modification of the Fe₃O₄/nHA by CPTES

2 g Fe₃O₄/nHA were premixed by ultrasonication in 100 ml of dried toluene. Then, 8 ml CPTES was added and the mixture was refluxed at 80°C for four days. The HA-coated nanoparticles were collected by an external magnet and washed with ethanol (3 ×) and acetone (3 ×) and then were dried at 50°C under a vacuum 24 h [7].

2.2.6. Preparation of Fe₃O₄/nHA/CS nanoparticles

At the first, 1.12 g of CS dissolve in 100 ml of 3% acetic acid and its mix by an alto-magnetic stirrer for 4 hours, then remove the magnet from the mixture, and dispersed by Ultrasonic bath for about 1 hour. Then, 4.8 g of powder Fe₃O₄/nHA add to the solution and stirring by the electric stirrer for 3 hours. Then, 0.1 M NaOH was added to the solution to reach pH 9-10 and stirred with an electric stirrer for 24 hours. And in the end, the synthetic compound is rinsed with distilled water several times by the help of a magnet, then dry in an oven at 40°C for 24 hours [23].

2.2.7. MTX loading on the nanocarrier

The binding of MTX to the composite is accomplished by an esterification reaction between the hydroxyl groups of MNP and the carboxylic acid group of MTX. First, 40 mg of MTX has dissolved in 10 ml DMSO and then 18.2 mg DCC was added as a carboxyl group activator in the presence of 0.54 mg DMAP. The mixture was stirred for 1 h and then 80 mg of nanocarrier was added up and the mix was shaken at 40°C for 24 hours. The resulting product was centrifuged (6000 rpm, 15 min) and then washed with DMSO, deionized water and acetone, and dried at vacuum at room temperature [7].

2.3. Characterization of nanoparticles

The prepared nanoparticles were characterized for particle size (PS), zeta potential (ZP), DSC, scanning electron microscopy (SEM), FTIR, XRD, VSM, percentage yield, and drug release studies.

2.3.1. Particle size measurement

The means particle size was determined by Particle Size Analyzer (PSA) Scatterscope1. The formulation of the MTX charged nanoparticles was diluted with deionized water to a corresponding scattering intensity. The cumulative method was used to help analyze the data, considering spherical particles. The findings were measured as the effective diameter, and the poly-dispersity index (PDI) was determined as the relative width of the distribution of particle size.

2.3.2. UV analysis of MTX content

UV/Vis spectrophotometer measured the amount of conjugated MTX. The absorbance value of the polymers was measured in DMSO at a wavelength of 303 nm. The amount of conjugated MTX was calculated from a calibration curve of MTX over the range of 5–100 µg/ml. A calibration curve for MTX was diagramed over a concentration range of 2–10 µg/ml. The calibration curve was achieved by measuring the concentration of MTX on the X-axis and Y-axis of their respective absorbance. The calibration details are listed in Table No. 1 and the calibration curve is an exhibit in Fig. 6.

2.3.3. Determination the amount of MTX on nanocarrier

The percentage yield was determined according to Equation 1.

$$(\%) \text{ percentage Yield} = \frac{\text{amount of filtered and dried nanoparticles}}{\text{amount of solids dispersed in the dispersed phase}} \times 100 \quad (1)$$

2.3.4. Determination of drug encapsulation efficiency

The product encapsulation performance of the composition of nanoparticles was obtained by extracting the MTX nanoparticles from the aqueous storage medium clear of MTX (Equation 2). In the present study, dialysis bag method was used to achieve a separation. Pour 20 ml of the nanoparticle into a dialysis bag and insert it into a Beakers. DMSO (50 ml) was added to the beakers to cover the entire dialysis bag. The Beakers was then shaken slowly for 30 minutes. The sample was then extracted from the

solution inside the dialysis bag and read by absorbance with a UV spectrophotometer at 303 nm. The difference between the total amount of the drug and the amount of Methotrexate in the supernatant was the actual amount of drug loaded in the nanoparticles (Equation 3).

$$\% \text{ Drug encapsulation Efficiency} = \frac{\text{mass of drug in nanocarrier}}{\text{mass of nanocarrier}} \times 100 \quad (2)$$

$$\% \text{ Drug Loading Efficiency} = \frac{\text{mass of drug in nanocarrier}}{\text{mass of nanocarrier}} \times 100 \quad (3)$$

2.3.5. *In vitro* drug release studies

The USP II solubilizer is used to facilitate dissolution testing and to maintain temperature and other dissolution conditions. 300 ml of saline phosphate buffer pH = 7.4 is used as the dissolution medium. During the whole test period (24 hours), the stirring rate of the device was kept constant at 100 rpm, and the dissolution ambient temperature at $37^{\circ}\text{C} \pm 0.2$. To perform the dissolution test, 20 mg of the nano-formulations were weighed and poured into each cell. Sampling is performed at 0.5, 1, 2, 3, 4, 5, 6, 12, 24 and 36 hours. The concentration of a dissolved drug is measured at different times. The concentration of Methotrexate is determined by UV spectrophotometer at 303 nm. The amount of MTX released in each sample was determined using a calibration curve; the reported values are averages of three replicates ($n = 3$). Results of *in vitro* drug release studies obtained were tabulated and shown graphically as the concentration of drug vs time.

2.3.6. Determination of zeta potential

The Nano Sight (NS500, Malvern Instruments Ltd, UK) has calculated the zeta potential of MTX nanoparticle formulations. The samples of MTX nanoparticles was prepared by diluting nanoparticles in double-distilled water and held in an electrophoretic cell to obtain the zeta potential.

2.3.7. Fourier transform infra-red spectroscopy (FTIR)

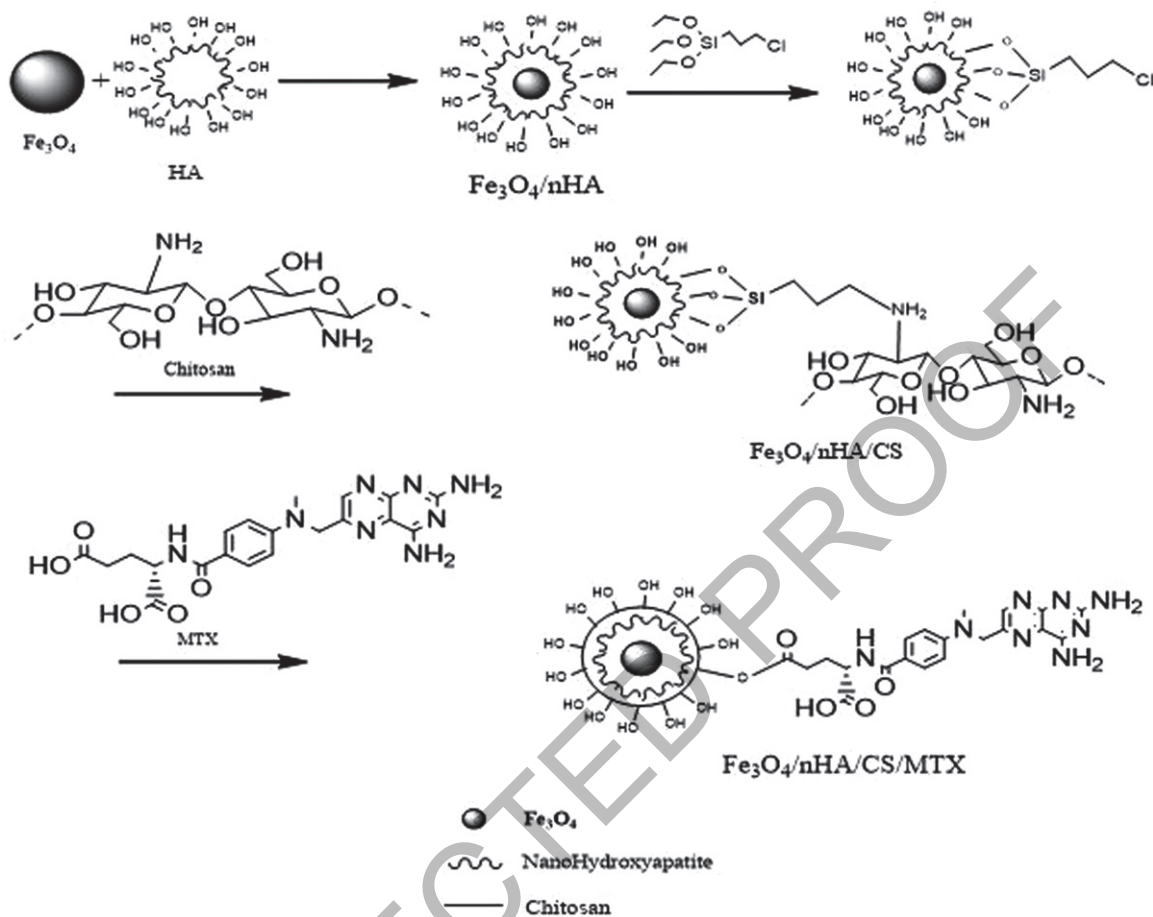
An FTIR-8400S spectrophotometer (Shimadzu, Japan) was used to evaluate the transmission spectra. The sample was prepared for examination by combining samples of pure product and nanoparticle (1 percent of the volume of potassium bromide) with potassium bromide powder. A hydraulic compression of 10000 psi primed the potassium bromide disk. More than 400–4000 cm^{-1} wavenumber regions were searched for the potassium bromide disk.

2.3.8. Scanning electron microscopy (SEM)

Scanning electron microscopy (JSM-T20, Kyoto, Japan) investigated the shape and surface characteristics of the nanoparticles. A fitting collection of nanoparticles was placed on metal (aluminum) stubs, utilizing double-sided carbon tape adhesive and broken with a razor blade. For secondary electron emissive SEM, the samples were sputter-coated with gold/palladium at 14 mA for 120 s under argon atmosphere and observed for morphology at 15 kV acceleration voltage.

2.3.9. Vibration Sample Magnetometer (VSM)

VSM-MDK6 was applied to determine the magnetic properties of $\text{Fe}_3\text{O}_4/\text{nHA}/\text{CS}$, nanocarrier, and SPIONs as a control sample. The field dependence and saturated nanocarrier magnetization were recorded under the circulating magnetic field in the range of $-1.5 - +1.5$ T at 300 K.

Scheme 1. Synthetic pathways in formation of $\text{Fe}_3\text{O}_4/\text{HA}/\text{Chitosan}/\text{MTX}$.

2.3.10. Differential scanning calorimeter (DSC)

The thermal properties of (2–3 mg) samples of the pure drug, $\text{Fe}_3\text{O}_4/\text{nHA}/\text{CS}$, and nanocarrier, as well as the prepared nano-formulation, was performed with a differential scanning calorimeter with indium (DC-60, Shimadzu, Japan). Samples were sealed in aluminum pans with lids and heated from 25 to 300°C at a rate of 10°C/min under nitrogen flow at a rate of 25 ml/min.

3. Results and discussion

3.1. Synthesis of magnetic nanocarrier

In this study, the magnetic nanocarrier was prepared in three steps as depicted in SCHEME 1. Afterward, MTX as a widely used anticancer drug was loaded to the nanocarrier. The examination of the FTIR spectra of the compounds prepared shows the correct reaction as shown in Fig. 2, The presence of 961 cm^{-1} peak corresponding to symmetric tensile bond P-O and 1038 cm^{-1} peak and 1091 cm^{-1} peak due to strong stretching absorption of PO_4 functional group and peaks appearing at m^{-1} and 3641 cm^{-1} , respectively the order of tensile vibrations of O-H shows the hydroxyapatite and water present in its system. The presence of 1384 cm^{-1} and 1637 cm^{-1} peaks is related to the carbonate functional group (C-O bond), indicating that some carbonate ions have been replaced by phosphate

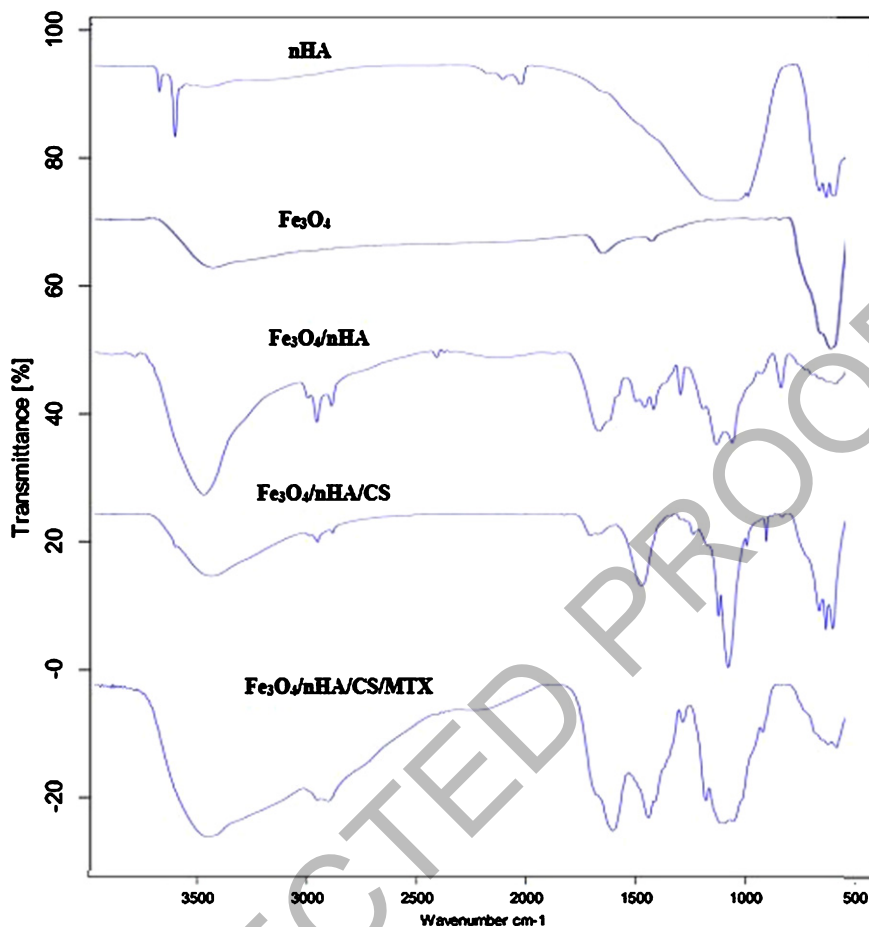


Fig. 2. FTIR spectra of (a) nHA, (b) Fe_3O_4 , (c) $\text{Fe}_3\text{O}_4/\text{nHA}$, (d) $\text{Fe}_3\text{O}_4/\text{nHA}/\text{CS}$ and (e) $\text{Fe}_3\text{O}_4/\text{nHA}/\text{CS}/\text{MTX}$.

ions in the apatite structure. Peaks at $700\text{-}500\text{ cm}^{-1}$ zones related to Fe-O bonding, sharp peaks at 582 cm^{-1} zones for tensile vibration Fe-O-Fe, two bands were seen at 1616 cm^{-1} , and 3389 cm^{-1} tensile and stretching absorption (O-H bonding) are hydroxyl groups, indicating proper synthesis of nanoparticles. In the spectrum of coated nanoparticles, the peaks of 1450 cm^{-1} and 1626 cm^{-1} are related to the hydroxyapatite carbonate functional group, and it is notable that the hydroxy peaks in the region of 3398 cm^{-1} are in the outer layer and are more clearly were seen. 442 cm^{-1} peak for Fe-O, 1090 cm^{-1} peak, and 1048 cm^{-1} peak for the PO_4 functional group present in the nanohydroxyapatite spectrum, which is also coated in the magnetic nanoparticles spectrum with a displacement value. Because of the interaction of these groups with each other. Peaks in the region of 1207 cm^{-1} are related to Si-O bonds, peaks in the region of 802 cm^{-1} are related to C-Cl, 3-chloropropyl bonds, 2851 cm^{-1} peaks, and 2920 cm^{-1} peaks. Alkane flexion and peak areas of 1443 cm^{-1} , 1639 cm^{-1} hydroxyapatite (C-O bond), and 3400 cm^{-1} hydroxy functional groups, which still indicate the remaining hydroxy alloy Hydroxysterines have not been functionalized and these peaks show a linker binding to the coated magnetic nanoparticles. In the spectrum of nanocarrier, Sharp peak at 1579 cm^{-1} for stretching uptake of the NH_2 functional group and peak at 1155 cm^{-1} for chitosan C-O bond, NH_2 , and OH groups were seen at 3423 cm^{-1} , indicating the addition of chitosan to magnetic nanocomposites in this area the spectrum of O-H magnetic nanocomposites is very weak and the bands of 2920 cm^{-1} and 2851 cm^{-1} are related to the magnetic alkanes group. The deletion of the peak at the 802 cm^{-1}

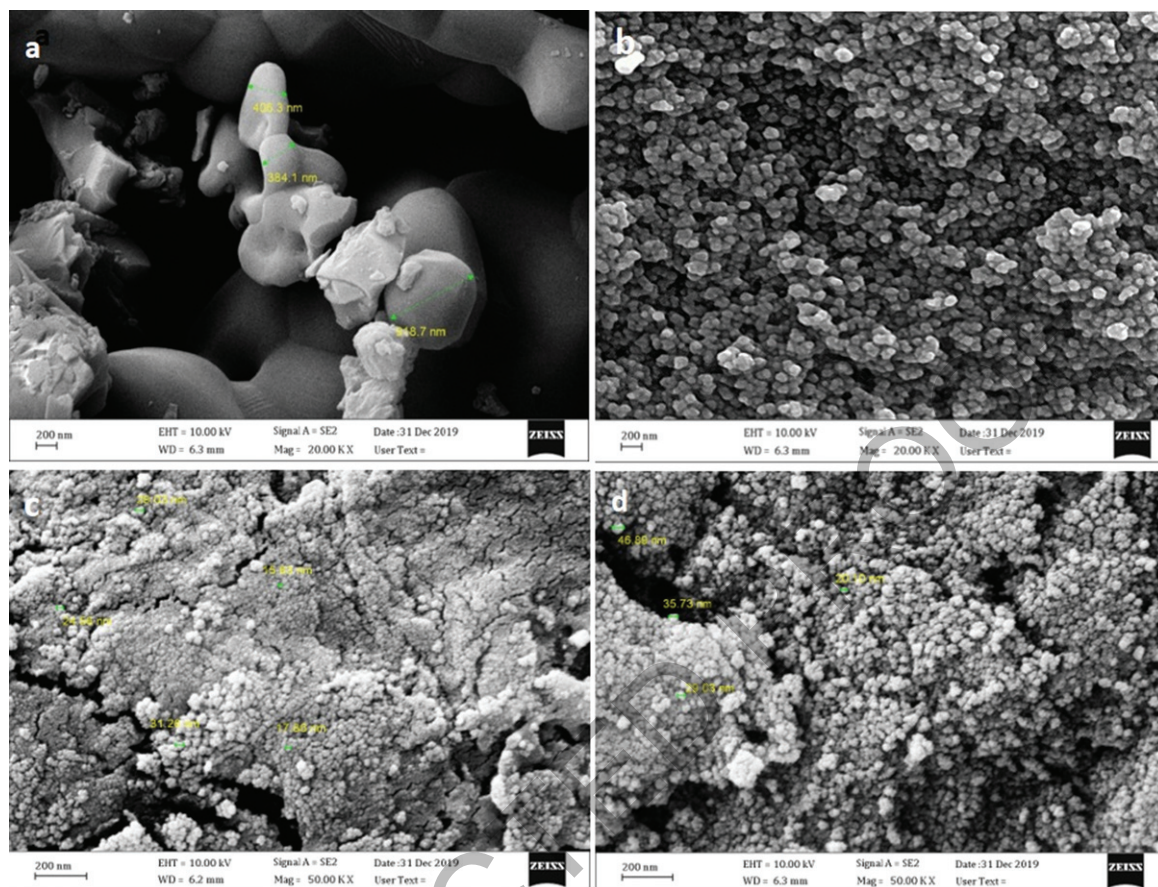


Fig. 3. SEM images of (a) nHA, (b) Fe_3O_4 , (c) $\text{Fe}_3\text{O}_4/\text{nHA}/\text{CS}$ and (d) $\text{Fe}_3\text{O}_4/\text{nHA}/\text{CS}/\text{MTX}$.

regions corresponding to the C-Cl linker shows the reaction. Existence of 1632 cm^{-1} peaks related to carbonyl amide, peaks in $1600\text{--}1400\text{ cm}^{-1}$ peaks related to Methotrexate gas ring, 1024 cm^{-1} peaks and 1096 cm^{-1} peaks corresponding to the hydroxyapatite PO_4 functional group and regions 2919 cm^{-1} and 2852 cm^{-1} assigned to alkanes as well as 3435 cm^{-1} nano-carrier peaks confirm that MTX has been successfully demonstrated on the magnetic nanocarrier surface.

3.2. Characterization of the magnetic nanocarrier

3.2.1. Scanning electron microscopy results of nanoparticles

The size and morphology of the nanoparticles were examined by field emission scanning electron microscopy at 200 nm and $1\text{ }\mu\text{m}$ (Fig. 3). By examining the images and considering their scale, it can be predicted that the size of the nanoparticles is between 30 nm and $1.5\text{ }\mu\text{m}$. The spherical shape of the nanoparticles and their size distribution is also confirmed by these images. Due to the dipole-dipole gravity force between the uncoated magnetic nanoparticles, the particles are stuck together, clustered, and eventually form larger particles. However, in the coated sample, the coating on the surface of the nanoparticles prevents the particles from adhering to each other, reducing the size of the nanoparticles. The reduction in particle size is meant to decrease the size of the magnetite core as the overall size of the coated nanoparticles increases due to the coating on their surface.

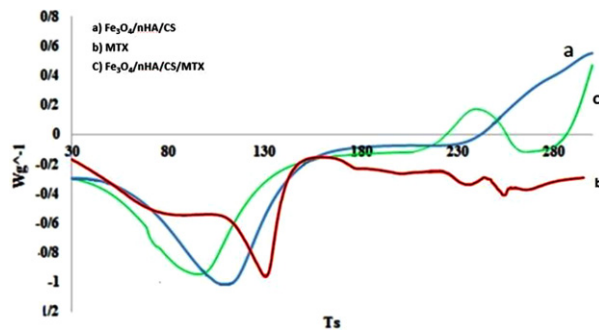


Fig. 4. DSC curves for pure Methotrexate, Fe₃O₄/nHA/CS, and Fe₃O₄/nHA/CS/MTX.

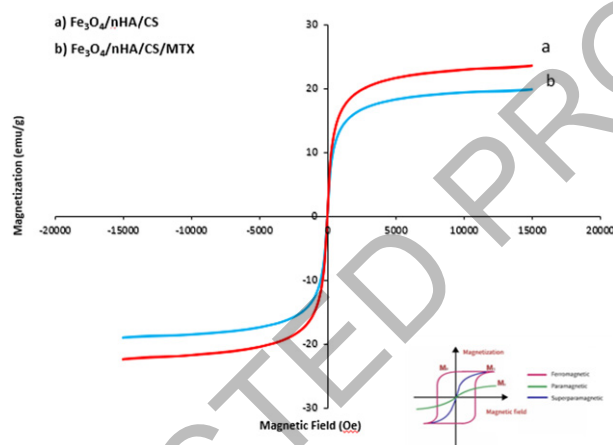


Fig. 5. Magnetization curves of (a) Fe₃O₄/nHA/CS, and (b) Fe₃O₄/nHA/CS/MTX.

3.2.2. Thermal analysis results of nanoparticles

DSC thermograms of Fe₃O₄/nHA/CS and MTX-loaded on Fe₃O₄/nHA/CS formulations are shown in Fig. 4. In this study, thermal analysis was performed using the DSC technique to investigate the placement of drug molecules and the mechanism of crystallization of nanoparticles in polymer substrates. Figure 4-a shows the thermal analysis chart of the magnetic nanocarrier, Fig. 4-b shows the Methotrexate drug, and Fig. 4-c shows the magnetic analysis chart of the nanocarrier of MTX. According to the available literature, pure Methotrexate melts at 220 °C, which occurs in Fig. 4 of the pure drug at about 240, indicating the presence of MTX in the nanocarrier and is crystalline and with a sharp peak. The drug represents the crystallinity of the drug, the drug has not changed physically, and the nanoparticles have remained crystalline and not amorphous.

3.2.3. Magnetic properties results of nanoparticles

The magnetic properties of the prepared Fe₃O₄/nHA/CS and MTX-loaded on Fe₃O₄/nHA/CS were analyzed by VSM at room temperature. The superparamagnetic behavior of the nanocarrier is shown in Fig. 5. According to the literature, the magnetization of more than 10 emu/g⁻¹ is usually appropriate for biomedical applications. Therefore, the saturated magnetization value of the Fe₃O₄/nHA/CS and MTX-loaded on Fe₃O₄/nHA/CS (Respectively, ~23 and ~19 emu/g⁻¹) represents a good magnetic character for biomedical applications. It has been reported that the decrease in the magnetization value of pure Fe₃O₄ (~49 emu/g⁻¹) is due to the existence of a large amount of polymer encapsulated the Fe₃O₄ nanoparticles. With the large saturation magnetization, the Fe₃O₄/nHA/CS could be separated

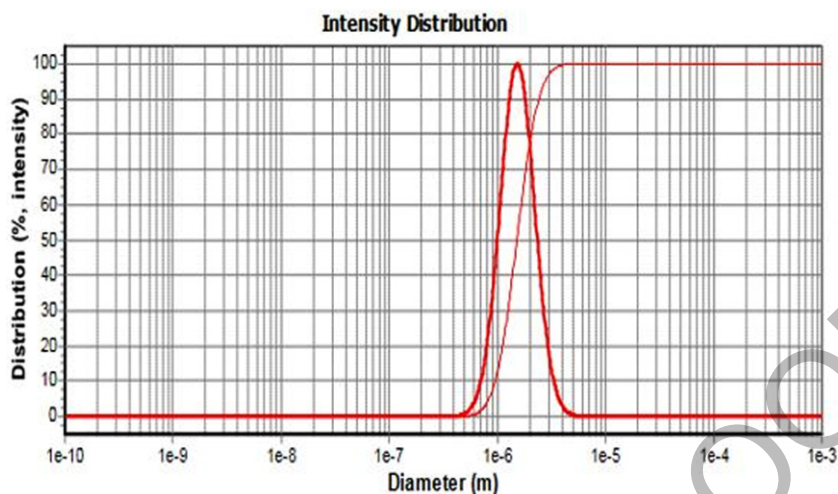


Fig. 6. PSA Results of Nanoparticles Prepared Using Desolvation Method.

from the medium rapidly and easily in the external magnetic field. The results show that the magnetic nanoparticle superparamagnetic nanoparticles and the Methotrexate carrier nanoparticles have lower magnetic properties than the Fe₃O₄ superparamagnetic nanoparticles because of the layer on which they are placed. The decrease in the magnetic property of Fe₃O₄ saturation is proportional to the thickness of the polymer coating on its surface so that the greater the coating thickness, the greater its magnetic property decreases.

3.2.4. Magnetic nanoparticle particle size results

Particle Size Analyzer (PSA) Scatteroscope1 was used to determine drug particle size, polymer, and formulations (Fig. 6). The samples are dispersed in distilled water (nanoparticles and polymers) or dimethyl sulfoxide (drug) and stirred continuously during the test. Each measurement was repeated three times. The average particle size of the magnetic nanoparticles was 1.5 μm . The nanoparticles polydispersity was calculated using $\text{PDI} = \delta^2 / (\text{mean})^2$ of 0.01 which is an acceptable value and the particles are close in size and this size helps to determine the pharmacokinetics. Predicts particles in the body and distributes them equally. The results showed that in all cases R^2 the regression equations were higher than the log-probability graphs and followed the logarithmic probability distribution.

3.2.5. Zeta potential results

The zeta potential of magnetic nanoparticles in aqueous solution is -16.4 mV in the aqueous solution, indicating high stability of the colloidal solution of these nanoparticles. Zeta potential is a measure of the stability of the particles in solution and the more positive or negative the value, the more stable the formulation. The magnetic zeta potential of the Methotrexate carrier in aqueous solution is -12.3 mV, indicating the effect of the drug on the nanocarrier which has made the nanoparticle zeta potential slightly more positive, which may be the drug itself. It has a positive charge that leads the nanocarrier to zero and a positive charge, which stabilizes the nanoparticles and decreases their stability (Fig. 7).

3.2.6. MTX loading and release studies

Concerning the study of the release of MTX from magnetic nanoparticles, our results showed that the release of MTX from magnetic nanoparticles was slow so that 7.5% of the drug was released from the nanoparticles within the first 3 hours but the release of MTX was slow and steady. 90% of the

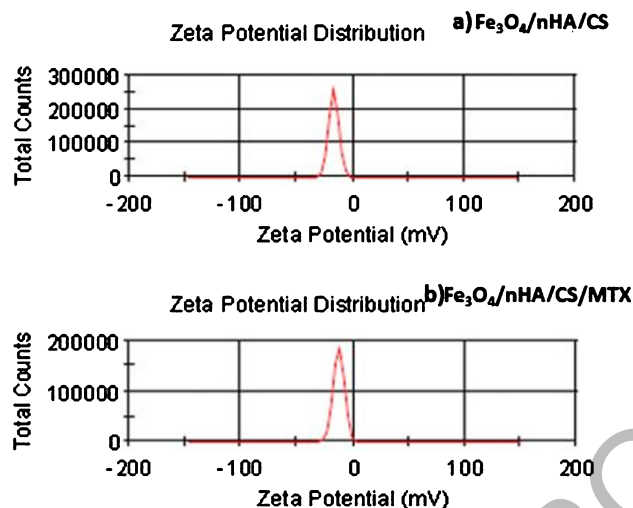


Fig. 7. zeta potential result of (a) $\text{Fe}_3\text{O}_4/\text{nHA}/\text{CS}$ and (b) $\text{Fe}_3\text{O}_4/\text{nHA}/\text{CS}/\text{MTX}$.

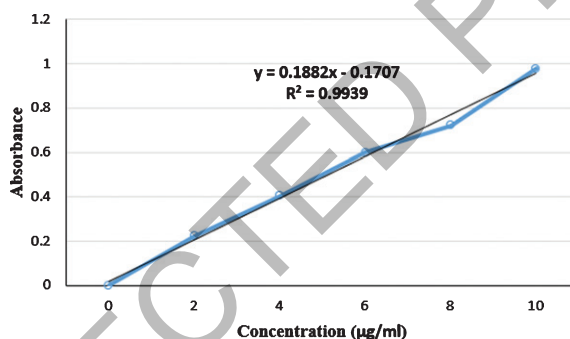


Fig. 8. Standard curve of Methotrexate UV absorption.

Table 1
Calibration Curve Data and Regression Values of Methotrexate

Order	1	2	3	4	5	6
Time (h)	0	2	4	6	8	10
Absorb device (nm)	0	0.2223 ± 0.0107	0.4041 ± 0.0053	0.5984 ± 0.0101	0.7218 ± 0.0173	0.9793 ± 0.0219

$n = 3$, all values \pm standard deviation.

drug was released within 36 hours. The rapid and explosive release of the drug from the nanoparticles can be related to the drug molecules that are located on the surface of the nanoparticles, and the slow release is due to the drug molecules located in the polymer matrix. Most *in vivo* biopolymers are mostly degraded by the enzyme. The hydrolysis of chitosan and its derivatives is generally carried out by lysosomes, chitonases, chitinases, and chitin deacetylase enzymes. A possible mechanism for the release of MTX loaded onto the nanocarrier is that the complex enters the cell via endocytosis through the receptor, where it is trapped by the lysosome and enzymatically degraded (Fig. 8, Table 1).

MTX was used as an anticancer drug with carboxylic acid groups to test the loading and controlled release behaviors of MTX and the capability for drug adsorption by MTX-loaded on nanocomposite as a nanocarrier. MTX may be loaded into nanocarriers by ionic interaction between the carboxylate

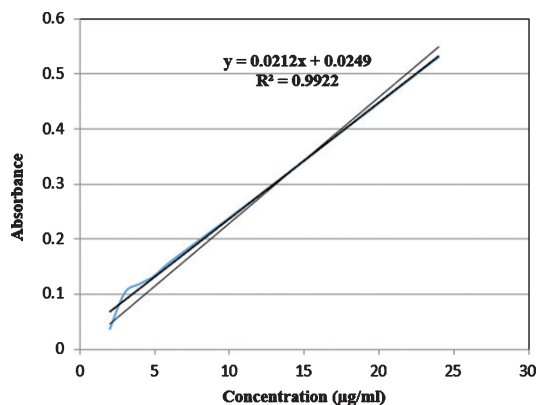


Fig. 9. Release profile of the MTX nanoparticles.

Table 2
In vitro drug release data

Order	1	2	3	4	5	6	7	8	9	10
Time(h)	0.5	1	2	3	4	5	6	12	24	36
Absorb device (nm)	0.01 ± 0.0005	0.013 ± 0.0009	0.037 ± 0.0026	0.103 ± 0.0037	0.119 ± 0.0051	0.134 ± 0.0082	0.158 ± 0.0095	0.28 ± 0.0111	0.53 ± 0.0132	0.83 ± 0.0163

$n = 3$, all values \pm standard deviation.

Table 3
Data Kinetics of drug release from magnetic nanocarriers

ORDER	RSQ	Slope	intercept	MPE%	K
Zero	0.98624	0.02807	0.0307805	279892	0.0280675
first	0.89511	-0.1044	0.2435502	2507152	-0.104393
Higuchi	0.95774	0.17588	-0.144946	1301756	0.1758761
peppas	0.9952	1.10097	-3.595141	19.4342	3.0070804
Hixon	0.97135	0.01982	-0.024726	691166	0.0198226
Square root of mass	0.9908	0.02369	-0.015666	287055	0.0236931
Three seconds root of mass	0.99793	0.02593	-0.001782	25	0.0259269
weibull	0.99326	1.15866	-3.373869	19.2873	0.0543741
Wagner Linear	0.71027	0.12895	-2.153959	142047	0.1289482
Wagner Logarithmic	0.80573	0.45299	-1.301781	112.792	0.4529887

anion of MTX and protonated amino groups of the nanocarrier at pH 7.4. The drug encapsulation efficiency (EE) and drug loading efficiency (LE) percentages of MTX in nanocarrier were 86.66 % and 28.8 %, respectively. The cumulative release of MTX is also shown in Fig. 9. We assume the simultaneous occurrence of both ionic and physical trapping has prevented the release of bursts or poor quality of product loads. Up to 92 % of MTX was released from the nanocarriers in physiological conditions (pH 7.4) after 36 hours (Fig. 8, Table 2).

3.2.7. Nanoparticle release kinetics mode

To investigate the kinetics of drug release, the models of zero degree, first degrees, Higuchi, the root of 1.2 mass, the root of mass 3.1, the root of mass 3.2, Weibull, Wagner linear, logarithmic Wagner and Peppas were obtained. The results of the studies are presented in Table 3, for these data for all

samples (zero degree, first degrees, Higuchi, etc.). Given their error percentage, which is less than the error rate of the Peppas equation, according to the results of the kinetics of the liberation equations, the Peppas equation shows that the mechanism is the controller of the diffusivity (Table 3).

4. Conclusion

In this study, the FTIR spectrum of calcium carbonate obtained from Sea Urchin shell and spine with its reference spectrum indicates that hydroxyapatite preparation from both is possible. Hydroxyapatite can be obtained from onshore and offshore sources (such as seaweed, starfish, coral, Sea urchin shell, etc.). *Echinometra mataei* was used in this project as one of the dominant indigenous species of Sea urchin on the southern coast of Iran. The kinetic pattern of drug release from the nanoparticles showed that the maximum amount of drug release corresponded to the root of Peppas. The FTIR results and the SEM images showed that the nanoparticles were synthesized and coated successfully and their size was in the range of 30 nm–1.5 μ m. It also reduces the aggregation or clotting of the nanoparticles, and the modified nanoparticles form a more stable suspension and lead to reduction in the size (diameter) of the nanoparticles. The reduction in particle size is meant to decrease the size of the magnetite core as the overall size of the coated nanoparticles increases due to the coating on their surface. Hydroxyapatite nanoparticles can bond with the chitosan amine group due to their Ca and PO₄ ions and cause the nanocarrier strength. The more positive the zeta potential of the magnetic nanoparticles showed the positive effect of the drug on the nanoparticles and their stability. The pure drug peak occurs at about 240, indicating the presence of MTX in the nanocarrier and is crystalline, and the sharp peak of the drug indicates that the drug is crystalline and the drug is physically unchanged and in the nanocarrier crystalline state. Remaining and not amorphous. Coating iron oxide nanoparticles with nanohydroxyapatite, and optimizing it with 3-(chloropropyl)triethoxysilane and chitosan, increased the possibility of covalent MTX interaction in magnetic nanoparticles, their stability, and biocompatibility and prevents the nanoparticles from accumulating or clotting and forms a more stable suspension. The present study demonstrates the potential of iron oxide nanoparticles in designing new magnetic nanoparticles and targeting them with other molecules for drug delivery and cancer chemotherapy.

Funding

This work financially supported by grant (MPSRC-9707) from Vice Chancellor for Research Affairs of Ahvaz Jundishapur University of Medical Sciences. This paper adapted from the thesis of Ali Rajabiyani.

References

- [1] N.A. Aval, J.P. Islamian, M. Hatamian, M. Arabfirouzjaei, J. Javadpour and M-R. Rashidi, Doxorubicin loaded large-pore mesoporous hydroxyapatite coated superparamagnetic Fe₃O₄ nanoparticles for cancer treatment, *International Journal of Pharmaceutics* **509**(1-2) (2016), 159–167.
- [2] L.K. Rahman and S.R. Chhabra, The chemistry of methotrexate and its analogues, *Medicinal Research Reviews* **8**(1) (1988), 95–155.
- [3] A. Lima, H. Sousa, J. Monteiro, R. Azevedo, R. Medeiros and V. Seabra, Genetic polymorphisms in low-dose methotrexate transporters: current relevance as methotrexate therapeutic outcome biomarkers, *Pharmacogenomics* **15**(12) (2014), 1611–1635.
- [4] B. Álvarez-González, M. Rozalen, M. Fernández-Perales, M.A. Álvarez and M. Sánchez-Polo, Methotrexate Gold Nanocarriers: Loading and Release Study: Its Activity in Colon and Lung Cancer Cells, *Molecules* **25**(24) (2020), 6049.

- [5] G. Choi, T-H. Kim, J-M. Oh and J-H. Choy, Emerging nanomaterials with advanced drug delivery functions; focused on methotrexate delivery, *Coordination Chemistry Reviews* **359** (2018), 32–51.
- [6] T. López, M. Alvarez, S. Arroyo, A. Sánchez, D. Rembao and R. López, Obtaining of SiO₂ nanostructured materials for local drug delivery of methotrexate, *J Biotechnol Biomaterial S* **4**(2) 2011.
- [7] F. Farjadian and S. Ghasemi, Mohammadi-Samani. Hydroxyl-modified magnetite nanoparticles as novel carrier for delivery of methotrexate, *International Journal of Pharmaceutics* **504**(1-2) (2016), 110–116.
- [8] M.D. Felisberto and M. Laranjeira, Preparation and characterization of hydroxyapatite-coated iron oxide particles by spray-drying technique, *Anais da Academia Brasileira de Ciências* **81**(2) (2009), 179–186.
- [9] J. Mamani, Ajd. Costa-Filho, D.R. Cornejo, E. Vieira and L. Gamarra, Synthesis and characterization of magnetite nanoparticles coated with lauric acid, *Materials Characterization* **81** (2013), 28–36.
- [10] M.G. Adimoolam, N. Amreddy, M.R. Nalam and M.V. Sunkara, A simple approach to design chitosan functionalized Fe₃O₄ nanoparticles for pH responsive delivery of doxorubicin for cancer therapy, *Journal of Magnetism and Magnetic Materials* **448** (2018), 199–207.
- [11] Y. Arum, Y-O. Oh, H.W. Kang, S-H. Ahn and J. Oh, Chitosan-coated Fe₃O₄ magnetic nanoparticles as carrier of cisplatin for drug delivery, *Fish Aquat Sci* **18**(1) (2015), 89–98.
- [12] S. Valizadeh, M. Rasoulifard and M.S. Dorraji, Modified Fe₃O₄-hydroxyapatite nanocomposites as heterogeneous catalysts in three UV, Vis and Fenton like degradation systems, *Applied Surface Science* **319** (2014), 358–366.
- [13] N.L. Ignjatović, K.M. Penov-Gaši, V.M. Wu, J.J. Ajduković, V.V. Kojić, D. Vasiljević-Radović, et al., Selective anti-cancer activity of hydroxyapatite/chitosan-poly (d, l)-lactide-co-glycolide particles loaded with an androstane-based cancer inhibitor, *Colloids and Surfaces B: Biointerfaces* **148** (2016), 629–39.
- [14] P. Oberbek, T. Bolek, A. Chlanda, S. Hirano, S. Kusnieruk, J. Rogowska-Tylman, et al., Characterization and influence of hydroxyapatite nanopowders on living cells, *Beilstein Journal of Nanotechnology* **9**(1) (2018), 3079–3094.
- [15] F. Heidari, M.E. Bahrololoom, D. Vashae and L. Tayebi, In situ preparation of iron oxide nanoparticles in natural hydroxyapatite/chitosan matrix for bone tissue engineering application, *Ceramics International* **41**(2) (2015), 3094–100.
- [16] A. Kroh and A.B. Smith, The phylogeny and classification of post-Palaeozoic echinoids, *Journal of Systematic Palaeontology* **8**(2) (2010), 147–212.
- [17] P. Delianis, The potency of sea urchin (*Diadema setosum*) gonad on brain cells of white rats (*Rattus norvegicus*), *Asian Journal of Pharmaceutics (AJP)* **10**(2) 2016.
- [18] C.A. Etensohn, Sea Urchins as a Model System for Studying Embryonic Development. 2017.
- [19] SAKA. Rahim and R. Nurhasan, Status of sea urchin resources in the East Coast of Borneo, *Journal of Marine Biology* **2016** 2016.
- [20] S.E. Naleway, J.R. Taylor, M.M. Porter, M.A. Meyers and J. McKittrick, Structure and mechanical properties of selected protective systems in marine organisms, *Materials Science and Engineering: C* **59** (2016), 1143–67.
- [21] H. Komalakrishna, T.S. Jyoth, B. Kundu, S. Mandal, Low Temperature Development of Nano-Hydroxyapatite from *Austrorhynchus psittacus*, Star fish and Sea urchin, *Materials Today: Proceedings* **4**(11) (2017), 11933–11938.
- [22] S. Mohapatra, S. Sahu, S. Nayak and S.K.J.L. Ghosh, Design of Fe₃O₄@SiO₂@carbon quantum dot based nanostructure for fluorescence sensing, magnetic separation, and live cell imaging of fluoride ion, *Langmuir* **31**(29) (2015), 8111–8120.
- [23] S.A. Moayedi, A. Teimouri and H. Salavati, Synthesis and Characteristics nanocomposites of MCSHA and MHACS and comparison of adsorption of methylene blue with adsorbents. Available at SSRN 3165206. 2018 Apr 18.